American Mineralogist, Volume 96, pages 1475–1479, 2011

A first-principles investigation of hydrous defects and IR frequencies in forsterite: The case for Si vacancies

Koichiro Umemoto,[1,*] Renata M. Wentzcovitch,[2,3] Marc M. Hirschmann,[1] David L. Kohlstedt,[1] and Anthony C. Withers[1]

[1]Department of Geology and Geophysics, University of Minnesota, 310 Pillsbury Drive SE, Minneapolis, Minnesota 55455, U.S.A.
[2]Department of Chemical Engineering and Materials Science, University of Minnesota, 421 Washington Ave SE, Minneapolis, Minnesota 55455, U.S.A.
[3]Minnesota Supercomputing Institute, University of Minnesota, 117 Pleasant Street SE, Minneapolis, Minnesota 55455, U.S.A.

Abstract

We investigate charge-balanced hydrous magnesium and silicon defects [$(2H)^{X}_{Mg}$, $(4H)^{X}_{Si}$] by first principles. Two new lowest-energy hydrogen configurations are proposed for $(4H)^{X}_{Si}$. With these new configurations, the distribution of O-H stretching phonon frequencies in Group I (>3450 cm^{-1}) are better reproduced. Substitution of silicon with four hydrogen atoms gives rise to significant elongation of distances between O atoms at the tetrahedron of the silicon vacancy. Our calculations indicate that the correlation between O-O distances and O-H stretching phonon frequencies, which has been well established for hydrous minerals, does not apply directly to nominally anhydrous minerals and should not be used to determine the identity of hydrous defects responsible for infrared absorption peaks.

Keywords: Hydrous defects, forsterite, phonon frequencies, nominally anhydrous minerals, first principles

Introduction

The physical properties of the Earth's upper mantle, whose main component is olivine, are strongly affected by trace amounts of water (for a review, see Keppler and Smyth 2006). Water is incorporated in the olivine structure as interstitial hydrogen, in some cases associated with another minor element, such as aluminum or ferric iron. Structures of hydrous defects, therefore, offer fundamental information about the nature and energies involved in processes related to the presence of water. Several computational first-principles studies, which looked into hydrous defects at the atomic scale, have investigated the formation energies of H associated with Mg and Si vacancies and at interstitial sites (Wright and Catlow 1994; Haiber et al. 1997; Brodholt and Refson 2000; Braithwaite et al. 2003; Walker et al. 2003, 2006, 2007; Verma and Karki 2009). Experimental documentation of the atomic structures of hydrous defects is not straightforward, but infrared (IR) spectroscopy of hydrous forsterite/olivine provides helpful information about O-H stretching modes. There are several IR studies of water-bearing forsterite/olivine (e.g., Bai and Kohlstedt 1992, 1993; Libowitzky and Beran 1995; Lemaire et al. 2004; Matsyuk and Langer 2004; Berry et al. 2005; Matveev et al. 2001, 2005; Koch-Müller et al. 2006; Kudoh et al. 2006; Mosenfelder et al. 2006; Smyth et al. 2006; Thomas et al. 2009; Gose et al. 2010; Kovacs et al. 2010) and these show that the IR spectra depend on silica activity influenced by buffer materials (periclase and enstatite) and the presence of metallic cations (iron, titanium, and so on). Absorption bands of IR spectra have been divided into two groups: Group I (phonon frequencies > 3450 cm^{-1}) and Group II (<3450 cm^{-1}) (Bai and Kohlstedt 1992, 1993). The Group I bands consist of multiple convoluted peaks. The origin of this complex profile has not been clear, but it is not likely from a single hydrogen configuration. Some experiments attributed these peaks to hydrous Si vacancies (Matveev et al. 2001; Berry et al. 2005; Kovacs et al. 2010) and hydrous Mg vacancies (Kudoh et al. 2006; Smyth et al. 2006). Others claimed that these peaks should be related to both Mg and Si vacancies (Lemaire et al. 2004; Koch-Müller et al. 2006; Gose et al. 2010). Kohlstedt (2006) also suggested, on the basis of solubility and diffusion constants, that the primary defects involved in incorporation of hydrogen in olivine should be Mg vacancies. Theoretically, the Group I bands were attributed to the Si defects (Braithwaite et al. 2003; Walker et al. 2006).

In the present paper, we reinvestigate hydrous defects associated with vacant Si and Mg sites in forsterite by first-principles calculations. We propose new hydrogen configurations for the hydrogen-saturated Si vacancy, $(4H)^{X}_{Si}$. These new configurations together are able to explain IR peaks in the Group I spectral region better than other configurations that have been previously considered. The new hydrogen configurations are expected to occur not only in forsterite but also in wadsleyite and ringwoodite, which also contain SiO_4 tetrahedra.

Computational method

Calculations were performed using the generalized gradient approximation (GGA) (Perdew et al. 1996). The pseudopotentials for Si, O, and H were generated by Vanderbilt's method (Vanderbilt 1990). The valence electronic configurations used are $3s^2 3p^2 3d^0$, $2s^2 2p^4$, and $1s^1$ for Si, O, and H, respectively. Core radii for all quantum numbers l are 1.6, 1.4, and 0.5 a.u. for Si, O, and H, respectively. The pseudopotential for Mg was generated by von Barth-Car's method (Karki et al. 2000). The planewave cutoff energy is 544 eV. Forsterite at 0 GPa with 28 atoms and no vacancies was optimized using variable-cell-shape molecular dynamics (Wentzcovitch 1991; Wentzcovitch et al. 1993) with the 4×2×4 k-point mesh. The optimized lattice constants of forsterite without vacancies are a = 4.800 Å,

* E-mail: umemo001@umn.edu

b = 10.293 Å, and c = 6.020 Å (for the *Pbnm* symmetry). To study vacancies, we generated a 2×1×2 supercell (consisting of 128 atoms in defect-free forsterite). The 2×2×2 k-point mesh is used for this supercell. In this supercell, we relaxed internal atomic coordinates with cell parameters fixed. Dynamical matrices for hydrogen atoms were computed at the Γ point using density-functional perturbation theory (Giannozzi et al. 1991; Baroni et al. 2001). All calculations were performed by using the Quantum-ESPRESSO software distribution (Giannozzi et al. 2009).

Results

New hydrogen configurations of $(4H)^{x}_{Si}$

For $(4H)^{x}_{Si}$, we find four distinct hydrogen configurations, configuration 1 to configuration 4 (Fig. 1; four CIFs are available on deposit[1]). Owing to the mirror symmetry plane perpendicular to the **c** axis in perfect forsterite, configurations 2 and 3 each have one additional equivalent configuration; the numbers of structural degeneracies are 1 for configurations 1 and 4, and 2 for configurations 2 and 3, respectively. Configurations 3 and 4 are similar to those found in previous studies (Brodholt and Refson 2000; Walker et al. 2007; Verma and Karki 2009) where the hydrogen bonded to O1 migrates to the exterior of the tetrahedron and the other three hydrogen atoms stay on the faces. Configuration 3 is also similar to the configuration reported by Walker et al. (2007). Configuration 4 is identical to the configuration reported by Brodholt and Refson (2000). The energy difference between configurations 3 and 4 is 0.1 eV. In contrast to the results of Brodholt and Refson (2000), configuration 4 has higher energy than configuration 3. This difference is caused by the use of different pseudopotentials, XC functionals, PBE-GGA vs. PW91-GGA, and k-point samplings adopted in our studies.

Configurations 1 and 2 are reported here for the first time as far as we know. In configuration 1, three hydrogen atoms bonded to O1 and two O3s are on tetrahedral edges and hydrogen bonded to O2 is outside the tetrahedron and pointing toward an interstitial site (I1), which is an inversion center. Configuration 2 corresponds to configuration 1 rotated by 120° about the **a** axis; three hydrogen atoms bonded to O1, O2, and one of two O3s are on tetrahedral edges and hydrogen bonded to another O3 is outside the tetrahedron and pointing toward another interstitial site (I2) on the mirror plane. Configuration 1 is the lowest-energy configuration. Configuration 2 has higher energy than configuration 1, but the energy difference, 0.022 eV, is very small. Energies of configurations 3 and 4 are higher than configuration 1 by 0.23 and 0.33 eV, respectively. The average distances between the four hydrogen atoms are 2.71, 2.62, 1.97, and 1.91 Å in configurations 1, 2, 3, and 4, respectively. Therefore, the configuration energy decreases as the average distance between hydrogen atoms increases. This result is reasonable, considering the repulsive nature of the Coulomb interaction between protons. Despite the small energy differences between configurations, at finite temperatures, these configurations should occur with different probabilities, p_i, given approximately by

$$p_i = w_i \exp\left(-\frac{E_i}{k_B T}\right) / Z, Z = \sum_{i=1}^{4} w_i \exp\left(-\frac{E_i}{k_B T}\right)$$

where w_i is the configurational degeneracy for the i-th configuration; $w_1 = w_3 = 1$ and $w_2 = w_4 = 2$. At 300 K, $p_1 = 0.54$ and $p_2 = 0.46$, while p_3 and p_4 are negligible. At 1500 K, $p_1 = 0.32$, $p_2 = 0.54$, $p_3 = 0.11$, and $p_4 = 0.02$. Probabilities of configurations 3 and 4 are small even at high temperatures that are relevant to the upper mantle.

[1] Deposit item AM-11-051, CIFs. Deposit items are available two ways: For a paper copy contact the Business Office of the Mineralogical Society of America (see inside front cover of recent issue) for price information. For an electronic copy visit the MSA web site at http://www.minsocam.org, go to the *American Mineralogist* Contents, find the table of contents for the specific volume/issue wanted, and then click on the deposit link there.

Table 1. Calculated O-H stretching mode frequencies (in cm^{-1})

$(4H)_{Si}$, conf. 1	3554, 3572, 3612, 3626
$(4H)_{Si}$, conf. 2	3433, 3525, 3541, 3589
$(4H)_{Si}$, conf. 3	3457, 3471 ,3519, 3681
$(4H)_{Si}$, conf. 4	3477, 3626, 3629, 3675
$(2H)_{Mg1}$	3186
$(2H)_{Mg2}$	3240, 3259

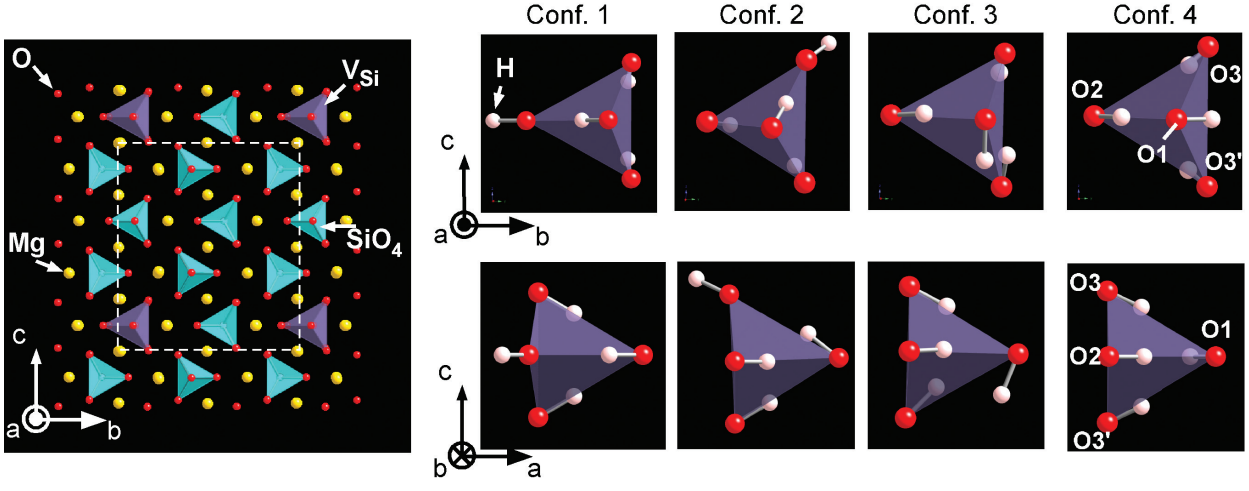

Figure 1. (left) Supercell of forsterite. **(right)** Four hydrogen configurations. Yellow, light blue, red, and white spheres denote magnesium, silicon, oxygen, and hydrogen atoms. (Color online.)

Vibrational density of states

Phonon frequencies of O-H stretching modes are calculated for all hydrogen configurations. Since there are four hydrogen atoms, there are four O-H stretching modes in each configuration. Calculated phonon frequencies, ω_j, are listed in Table 1. Vibrational density of states (VDOS) for the *i*-th configuration is estimated by summing Gaussian functions with FWHM of 20 cm^{-1} centered at ω_j (j = 1–4) (Figs. 2a–2d). At finite temperatures, the statistical average of VDOS is obtained by adding VDOSs of all configurations weighted by probabilities p_i. Figures 2e and 2f show VDOS at 1500 K with and without configurations 1 and 2. Calculated VDOSs do not correspond directly to experimental IR spectra, because VDOSs are not weighted by the IR scattering cross section. Figures 2e and 2f indicate that the calculated VDOS at 1500 K from all configurations agrees better with experimental spectra (Kovacs et al. 2010) than the VDOS without configurations 1 and 2. The presence of configurations 1 and 2 naturally explains several peaks and their widespread distribution in the Group I frequency region. Without configurations 1 and 2, peaks in Group I are further separated into two groups with a frequency interval between them, making the VDOS rather different from the experimental spectrum. This agreement supports the existence of configurations 1 and 2 for the hydrous silicon vacancy $(4H)^{X}_{Si}$. Therefore, our results attribute the multiple IR bands in the Group I region to the simultaneous presence of several $(4H)^{X}_{Si}$ configurations. This result contrasts with findings by Walker et al. (2006). Those authors proposed that the coexistence of one $(4H)^{X}_{Si}$ plus other differently charged hydrous defects, $(OH)^{\bullet}_{O3}$ (i.e., interstitial hydrogen bonded to O3), $(4H)^{X}_{Si}$, $(3H)'_{Si}$, and $(2H)''_{Si}$ could be the origin of the complex structure of IR spectra in the Group I region. However, silicon vacancies saturated by four hydrogen atoms are energetically substantially more favored. Reactions of hydrogen incorporations of $(OH)^{\bullet}_{O3}$ into $(3H)'_{Si}$ and $(2H)''_{Si}$ were calculated to be exothermic (Brodholt and Refson 2000; Verma and Karki 2009). In contrast, our model does not require the presence of unsaturated hydrous defects and explains reasonably well the origin of the multiple IR bands in the Group I region in hydrous forsterite annealed in wet condition.

In all $(4H)_{Si}$ configurations, most of O-H bonds are strongly aligned along the **a** axis. In all O-H bonds except for O2-H in configuration 1 and O1-H in configuration 4, *a* components are larger than *b* and *c* ones; in O2-H in configuration 1 and O1-H in configuration 4, *b* components are slightly larger than *a* ones. Therefore, these configurations support the pleochroic behavior observed experimentally, i.e., the largest absorption along the *a* axis in the Group I bands (Libowitzky and Beran 1995, Lemaire et al. 2004; Koch-Müller et al. 2006; Smyth et al. 2006; Thomas et al. 2009).

For the hydrous Mg vacancy, in the lowest-energy configuration, two hydrogen atoms are bonded to O2 atoms and sit nearly along the O2-O1 edges at the Mg1 vacancy, consistent with previous studies (Brodholt and Refson 2000; Braithwaite et al. 2003; Walker et al. 2006, 2007; Verma and Karki 2009). The IR-active O-H stretching mode frequency is 3186 cm^{-1}, similar

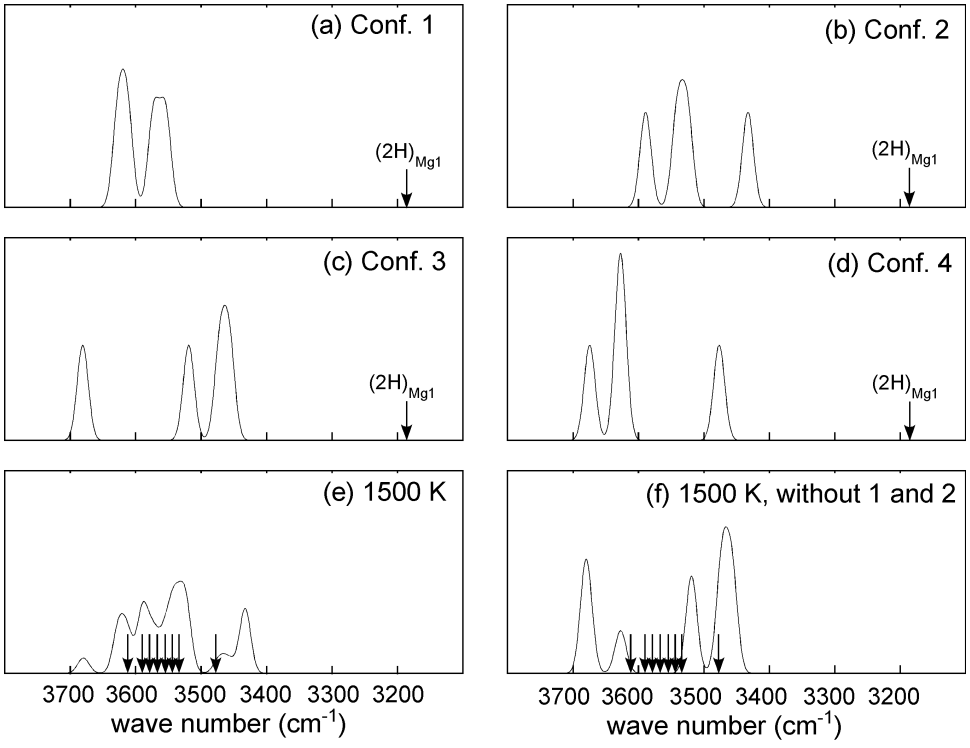

Figure 2. (**a**–**d**) Vibrational density of states (VDOS) calculated statically for configurations 1–4 of $(4H)_{Si}$. Arrows at 3186 cm^{-1} denote calculated phonon frequencies of $(2H)_{Mg1}$. (**e**) Statistical average of VDOS of all four configurations at 1500 K, (**f**) statistical average of VDOS of only configurations 3 and 4 at 1500 K. In **e** and **f**, arrows represent experimental major absorption bands of a sample labeled "p(15_1100)" by Kovacs et al. (2010).

to the previous result by Braithwaite et al. (2003) and Walker et al. (2006). The orientation of the H-O2 bond nearly parallel to the **c** axis is consistent with observations by polarized IR experiments showing that the Group II bands have highest intensity parallel to the **c** axis (Lemaire et al. 2004; Thomas et al. 2009). On the other hand, the hydrous Mg2 vacancy is less stable than the analogous Mg1 vacancy by 0.54 eV. O-H stretching mode frequencies in the Mg2 vacancy are 3240 and 3259 cm^{-1}, slightly higher than those in the Mg1 vacancy. This result is consistent with a suggestion by Lemaire et al. (2004) that the 3160 cm^{-1} band is related to the Mg1 site and the 3220 cm^{-1} band is related to the Mg2 site. On the other hand, hydrous Mg2 vacancies should be much less abundant than those at the Mg1 site, as they have considerably higher energy.

Combining results for $(4H)^{X}_{Si}$ and $(2H)^{X}_{Mg}$, it appears that Group I bands in IR spectra are related to Si vacancies and Group II bands are related to Mg vacancies. This outcome may at first seem strange, considering the well-known correlation between O-H stretching mode frequencies and O-O distances in minerals, whereby longer O-O distances are associated with higher O-H stretching mode frequencies (Libowitzky 1999). However, the correlation between O-O distances and O-H stretching frequencies was established for hydrous minerals, not for hydrous defects in nominally anhydrous minerals. In defect-free forsterite, i.e., forsterite without vacancies or hydrogen, O-O distances at the tetrahedral Si site are shorter than those at the octahedral Mg1 site. But this case does not apply when there are vacancies, as shown in Table 2. When Si and Mg sites are vacant, O-O distances of tetrahedral and octahedral edges increase, but relatively much more so for the Si vacancy (tetrahedral) site than for the Mg (octahedral) vacancy site. The net effect of these relaxations is to produce larger O-O distances in the Si vacancy site. This happens because Si-O bonds are much stronger than Mg-O bonds. In hydrous defects, the lengths of O-O edges at $(4H)^{X}_{Si}$ (2.981–3.196 Å), along which a hydrogen exists, are still longer than those at $(2H)^{X}_{Mg}$ (2.861 Å). Therefore, covalent O-H distances at $(4H)^{X}_{Si}$ (0.98–0.99 Å) are shorter than those at $(2H)^{X}_{Mg1}$ (1.01 Å). Shorter covalent O-H bond lengths result in higher O-H stretching frequencies. Therefore, the relationship between calculated O-H stretching mode frequencies and O-O and O-H distances for $(4H)^{X}_{Si}$ and $(2H)^{X}_{Mg}$ defects is quite reasonable and consistent with the correlations found by Libowitzky (1999), but this is not an obvious result. Kudoh et al. (2006) and Smyth et al. (2006) assigned the sharp Group I absorption bands in IR spectra to hydrogen atoms at the Mg site, based on site occupancies and O-O distances determined by X-ray diffraction (XRD) measurements. The experimental lengths of O-O tetrahedral edges at the Si sites in hydrous forsterite by a XRD measurement are 2.55–2.76 Å (Kudoh et al. 2006) and are almost equal to those in defect-free forsterite (Fujino et al. 1981). However, it is quite difficult to detect local elongation of O-O distances of tetrahedral edges at $(4H)^{X}_{Si}$ sites by XRD measurements, because oxygen positions and O-O distances are averaged over many $(Si)^{X}_{Si}$ sites and few $(4H)^{X}_{Si}$ sites. Our calculations indicate that it is inappropriate to correlate O-O distances in defect-free anhydrous minerals with O-H stretching mode frequencies of hydrous defects.

Elongation of O-O distances on tetrahedral edges is seen also experimentally in the hydrogarnet substitution between grossular [$Ca_3Al_2(SiO_4)_3$] and Si-free katoite [$Ca_3Al_2(O_4H_4)_3$]. In this hydrogarnet substitution, the average O-O distance increases by ~19%; in grossular and Si-free katoite, experimental average O-O distances on the tetrahedral edge are 2.69 and 3.18 Å, respectively (Novak and Gibbs 1971; Lager et al. 1987). For the solid solution of grossular and Si-free katoite, Lager et al. (1989) proposed a split-atom model in which oxygen positions are described in terms of two sites corresponding to those of grossular and Si-free katoite. Our calculations clearly support this model. In hydrogen-bearing coesite, IR measurements combined with the relationship by Libowitzky (1999) suggested that O-O distances at a $(4H)_{Si}$ defect should be larger than the O-O

TABLE 2. Structural data for tetrahedral and octahedral sites, calculated statically at 0 GPa

Tetrahedral site	Si_{Si}	V''''_{Si}	$(4H)_{Si}$, conf. 1	$(4H)_{Si}$, conf. 2	$(4H)_{Si}$, conf. 3	$(4H)_{Si}$, conf. 4
O-O distance (Å)						
O1-O2	2.798	3.531	3.196	3.023	2.993	2.992
O1-O3	2.803	3.446	2.999	3.088	2.981	3.024
O1-O3′	2.803	3.446	2.999	3.003	3.020	3.024
Covalent O-H bond length (Å)						
O1-H			0.983	0.986	0.989	0.979
O2-H			0.985	0.986	0.989	0.989
O3-H			0.985	0.992	0.990	0.982
O3′-H			0.985	0.987	0.979	0.982
Hydrogen-bond O···H length (Å)						
between O1 and O2			2.215	2.041	2.009	2.003
between O1 and O3			2.022	2.122	1.995	2.081
between O1 and O3′			2.022	2.017	2.127	2.082
O-H···O angle (°)						
O1-H-O2			175.3	174.1	173.3	180.0
O1-H-O3			170.7	165.9	173.8	160.4
O1-H-O3′			170.7	177.1	150.9	160.3

Octahedral site	Mg_{Mg}	V''_{Mg1}	$(2H)_{Mg1}$
O-O distance (Å)			
O1-O2	3.045	3.263	2.861
Covalent O-H bond length (Å)			
O2-H			1.007
Hydrogen-bond O···H length (Å)			
between O1 and O2			1.933
O-H···O angle (°)			
O1···H-O2			151.8

distance in coesite without hydrogen (Koch-Müller et al. 2003), being consistent with the present results.

ACKNOWLEDGMENTS

This work was supported by NSF/EAR 075903 and NSF/ATM 0428774. Computations were performed at the Minnesota Supercomputing Institute.

REFERENCES CITED

Bai, Q. and Kohlstedt, D.L. (1992) Substantial hydrogen solubility in olivine and implications for water storage in the mantle. Nature, 357, 672–674.

——— (1993) Effects of chemical environment on the solubility and incorporation mechanism for hydrogen in olivine. Physics and Chemistry of Minerals, 19, 460–471.

Baroni, S., de Gironcoli, S., Dal Corso, A., and Giannozzi, P. (2001) Phonons and related crystal properties from density-functional perturbation theory. Reviews of Modern Physics, 73, 515–562.

Berry, A.J., Hermann, J., O'Neill, H.S.C., and Foran, G.J. (2005) Fingerprinting the water site in mantle olivine. Geology, 33, 869–872.

Braithwaite, J.S., Wright, K., and Catlow, C.R.A. (2003) A theoretical study of the energetics and IR frequencies of hydroxyl defects in forsterite. Journal of Geophysical Research, 108, 2284.

Brodholt, J.P. and Refson, K. (2000) An ab initio study of hydrogen in forsterite and a possible mechanism for hydrolytic weakening. Journal of Geophysical Research, 105, 18977–18982.

Fujino, K., Sasaki, S., Takeuchi, Y., and Sadanaga, R. (1981) X-ray determination of electron distributions in forsterite, fayalite, and tephroite. Acta Crystallographica, B37, 513–518.

Giannozzi, P., de Gironcoli, S., Pavone, P., and Baroni, S. (1991) Ab initio calculation of phonon dispersions in semiconductors. Physical Review B, 43, 7231–7242.

Giannozzi, P., Baroni, S., Bonini, N., Calandra, M., Car, R., Cavazzoni, C., Ceresoli, D., Chiarotti, G.L., Cococcioni, M., Dabo, I., and others. (2009) Quantum ESPRESSO: A modular and open-source software project for quantum simulations of materials. Journal of Physics: Condensed Matter, 21, 395502.

Gose, J., Schmädicke, E., Markowitz, M., and Beran, A. (2010) OH point defects in olivine from Pakistan. Mineralogy and Petrology, 99, 105–111.

Haiber, M., Ballone, P., and Parrinello, M. (1997) Structure and dynamics of protonated Mg_2SiO_4: An ab-initio molecular dynamics study. American Mineralogist, 82, 913–922.

Karki, B.B., Wentzcovitch, R.M., de Gironcoli, S., and Baroni, S. (2000) High-pressure lattice dynamics and themoelasticity of MgO. Physical Review B, 61, 8793–8800.

Keppler, H. and Smyth, J.R., Eds. (2006) Water in Nominally Anhydrous Minerals, vol. 62. Reviews of Mineralogy and Geochemistry, Mineralogical Society of America, Chantilly, Virginia.

Koch-Müller, M., Dera, P., Fei, Y., Reno, B., Sobolev, N., Hauri, E., and Wysoczanski, R. (2003) OH^- in synthetic and natural coesite. American Mineralogist, 88, 1436–1445.

Koch-Müller, M., Matsyuk, S.S., Rhede, D., Wirth, R., and Khisina, N. (2006) Hydroxyl in mantle olivine xenocrysts from the Udachnaya kimberlite pipe. Physics and Chemistry of Minerals, 33, 276–287.

Kohlstedt, D.L. (2006) The role of water in high-temperature rock deformation. In H. Keppler and J.R. Smyth, Eds., Water in Nominally Anhydrous Minerals, 62, p. 377–396. Reviews of Mineralogy and Geochemistry, Mineralogical Society of America, Chantilly, Virginia.

Kovacs, I., O'Neill, H.St.C., Hermann, J., and Hauri, E.H. (2010) Site-specific infrared O-H absorption coefficients for water substitution into olivine. American Mineralogist, 95, 292–299.

Kudoh, Y., Kuribayashi, T., Kagi, H., and Inoue, T. (2006) Cation vacancy and possible hydrogen positions in hydrous forsterite, $Mg_{1.985}Si_{0.993}H_{0.06}O_4$, synthesized at 13.5 GPa and 1300 °C. Journal of Mineralogical and Petrological Sciences, 101, 265–269.

Lager, G.A., Armbruster, T., and Faber, J. (1987) Neutron and X-ray diffraction study of hydrogarnet $Ca_3Al_2(O_4H_4)_3$. American Mineralogist, 72, 756–765.

Lager, G.A., Armbruster, T., Rotella, F.J., and Rossman, G.R. (1989) OH substitution in garnets: X-ray and neutron diffraction, infrared, and geometric-modeling studies. American Mineralogist, 74, 840–851.

Lemaire, C., Kohn, S.C., and Brooker, R.A. (2004) The effect of silica activity on the incorporation mechanisms of water in synthetic forsterite: A polarized infrared spectroscopic study. Contributions to Mineralogy and Petrology, 147, 48–57.

Libowitzky, E. (1999) Correlation of O-H stretching frequencies and O-H···O hydrogen bond lengths in minerals. Monatshefte für Chemie, 130, 1047–1059.

Libowitzky, E. and Beran, A. (1995) OH defects in forsterite. Physics and Chemistry of Minerals, 22, 387–392.

Matsyuk, S.S. and Langer, K. (2004) Hydroxyl in olivines from mantle xenoliths in kimberlites of the Siberian platform. Contributions to Mineralogy and Petrology, 147, 413–437.

Matveev, S., O'Neill, H.St.C., Ballhaus, C., Taylor, W.R., and Green, D.H. (2001) Effect of silica acitivity on OH^- IR spectra of olivine: Implications for low-$a$$SiO_2$ mantle metasomatism. Journal of Petrology, 42, 721–729.

Matveev, S., Portnyagin, M., Ballhaus, C., Brooker, R., and Geiger, C.A. (2005) FTIR spectrum of phenocryst olivine as an indicator of silica saturation in magmas. Journal of Petrology, 46, 603–614.

Mosenfelder, J.L., Deligne, N.I., Asimov, P.D., and Rossman, G.R. (2006) Hydrogen incorporation in olivine from 2–12 GPa. American Mineralogist, 91, 285–294.

Novak, G.A. and Gibbs, G.V. (1971) The crystal chemistry of the silicate garnets. American Mineralogist, 56, 791–825.

Perdew, J.P., Burke, K., and Ernzerhof, M. (1996) Generalized gradient approximation made simple. Physical Review Letters, 77, 3865–3868.

Smyth, J.R., Frost, D.J., Nestola, F., Holl, C.M., and Bromiley, G. (2006) Olivine hydration in the deep upper mantle: Effects of temperature and silica activity. Geophysical Research Letters, 33, L15301.

Thomas, S.M., Koch-Müller, M., Reichart, P., Rhede, D., Thomas, R., Wirth, R., and Matsyuk, S. (2009) IR calibrations for water determination in olivine, r-GeO_2, and SiO_2 polymorphs. Physics and Chemistry of Minerals, 36, 489–509.

Vanderbilt, D. (1990) Soft self-consistent pseudopotentials in a generalized eigenvalue formalism. Physical Review B, 41, 7892–7895.

Verma, A.K. and Karki, B.B. (2009) Ab initio investigations of native and protonic point defects in Mg_2SiO_4 polymorphs under high pressure. Earth and Planetary Science Letters, 285, 140–149.

Walker, A.M., Wright, K., and Slater, B. (2003) A computational study of oxygen diffusion in olivine. Physics and Chemistry of Minerals, 30, 536–545.

Walker, A.M., Demouchy, S., and Wright, K. (2006) Computer modeling of the energies and vibrational properties of hydroxyl groups in α- and β-Mg_2SiO_4. European Journal of Mineralogy, 18, 529–543.

Walker, A.M., Hermann, J., Berry, A.J., and O'Neill, H.St.C. (2007) Three water sites in upper mantle olivine and the role of titanium in the water weakening mechanism. Journal of Geophysical Research, 112, B05211.

Wentzcovitch, R.M. (1991) Invariant molecular-dynamics approach to structural phase transitions. Physical Review B, 44, 2358–2361.

Wentzcovitch, R.M., Martins, J.L., and Price, G.D. (1993) Ab initio molecular dynamics with variable cell shape: Application to $MgSiO_3$. Physical Review Letters, 70, 3947–3950.

Wright, K. and Catlow, C.R.A. (1994) A computer simulation study of (OH) defects in olivine. Physics and Chemistry of Minerals, 20, 515–518.

MANUSCRIPT RECEIVED OCTOBER 11, 2010
MANUSCRIPT ACCEPTED MAY 9, 2011
MANUSCRIPT HANDLED BY ALEXANDRA FRIEDRICH